Postprint of: Klimczuk T., Shick A., Khmelevskyi S., Kozub A., Kolincio K., Griveau J., Colineau E., Eloirdi R., Caciuffo R.: Structural and physical characterization of NpPt2In7. JOURNAL OF ALLOYS AND COMPOUNDS. Vol. 768 (2018), pp. 852-858. DOI: 10.1016/j.jallcom.2018.07.163

Structural and physical characterization of $NpPt_2In_7$

T. Klimczuk[a], A. B. Shick[b], S. Khmelevskyi[c], A.L. Kozub[a,b],
K.K. Kolincio[a], J.-C. Griveau[d], E. Colineau[d], R. Eloirdi[d], R. Caciuffo[d]

[a]*Faculty of Applied Physics and Mathematics, Gdansk University of Technology, Narutowicza 11/12, 80-233 Gdansk, Poland*
[b]*Institute of Physics, Czech Academy of Sciences, Na Slovance 2, 182 21 Prague, Czech Republic*
[c]*Center for Computational Materials Science, Vienna University of Technology, Wiedner Hauptstrasse 8-10, A-1040, Vienna, Austria*
[d]*European Commission, JRC, Directorate for Nuclear Safety and Security, Postfach 2340, 76125 Karlsruhe, Germany*

Abstract

A new neptunium intermetallic compound, $NpPt_2In_7$, has been synthesized in polycrystalline form and characterized by several macroscopic techniques. A Rietveld analysis of its powder x-ray diffraction pattern shows that $NpPt_2In_7$ crystallizes in a tetragonal lattice with $I4/mmm$ symmetry and lattice parameters a = 4.58471(3) Å, c = 21.5065(3) Å. Magnetic susceptibility, electrical resistivity, Hall effect, and heat capacity measurements indicate a metallic character and the occurrence of antiferromagnetic order below a Néel temperature T_N = 23 K. The transition is exceptionally robust and T_N decreases by 0.2 K under a magnetic field of 9 T. A modified Curie-Weiss fit of the high-temperature magnetic susceptibility curve $\chi(T)$ gives an effective magnetic moment $\mu_{eff} = 2.54\,\mu_B$ close to the value expected for trivalent Np. Low temperature heat capacity measurements give a reduced Sommerfeld linear coefficient close to 25 mJ $mol^{-1}.K^{-2}$ and a Debye Temperature Θ_D=181 K. First principles, correlated-band electronic structure calculations suggest that the neptunium magnetic moment in $NpPt_2In_7$ is localized and that a quasi-two-dimensional antiferromagnetic structure could result from the competition of very weak interlayer interactions leading to very anisotropic properties.

1. Introduction

The layered intermetallic family of compounds $A_nM_mIn_{3n+2m}$ (where M is a transition metal Co, Rh, Ir, Pd, or Pt and A is Ce, U, Np, or Pu) has been the object of wide attention during the past two decades because some of its cerium- and plutonium-based heavy-fermion members exhibit unconventional superconductivity in presence of magnetism [1, 2, 3, 4, 5, 6]. Here, we report the results of an extensive investigation of a newly synthesized member of the family, $NpPt_2In_7$.

Typically, Np-based compounds exhibit a non-superconducting, magnetically ordered ground state, as the electrons in the Np $5f$ shell are usually too localized for forming Cooper pairs. Examples are given by members of the $A_nM_mIn_{3n+2m}$ system, such as $NpCoGa_5$ [7, 8], $NpRhGa_5$ [9], and $NpPtGa_5$ [10]. Until now, only two Np-based superconductors have been reported: $NpPd_5Al_2$, a heavy-fermion d-wave superconductor with T_c = 4.9 K [11, 12, 13, 14] and $NpMo_6Se_8$ with T_c = 5.6 K [15]. Investigating novel layered intermetallic compounds of neptunium is therefore interesting for making progress in the rationalization of the interplay between magnetism and superconductivity in correlated $5f$-electron materials.

A Rietveld analysis of the X-ray diffraction pattern shows that $NpPt_2In_7$ is an isostructural analogue of $CePt_2In_7$ [16], which becomes a heavy fermion superconductor when compressed [17], and of the heavy-fermion paramagnet $PuPt_2In_7$ [18]. The physical properties of $NpPt_2In_7$ have been investigated by magnetic susceptibility, heat capacity and resistivity measurements. The results indicate the onset of antiferromagnetic (AF) order at T_N = 23 K. Experimental data are complemented by electronic structure calculations based on the correlated extension of the density functional theory (DFT+U), where Coulomb and exchange correlations, U and J, are added to the f-shell. The results of the calculations suggest that the investigated compound could be a realization of a local-moment quasi-two-dimensional AF metal.

Email address: tomasz.klimczuk@pg.edu.pl (T. Klimczuk)

2. Experimental details

A small (approx. 300 mg) polycrystalline sample of $NpPt_2In_7$ was synthesized by the arc-melting technique under zirconium gettered ultra pure atmosphere. Constituent elements of purity 99.9% or higher were used in the atomic ratio 1:2:7.2 (Np:Pt:In). A small excess of indium was used to compensate its evaporation during melting. The sample was remelted three times to improve homogeneity and then it was wrapped in tantalum foil, sealed in an evacuated quartz ampoule and put in a furnace at 500 °C for 4 weeks, before being furnace quenched to room temperature.

Room temperature powder X-ray diffraction (PXRD) studies were conducted on a Bruker D8 Focus diffractometer (CuKα source). To avoid contamination, a small amount of $NpPt_2In_7$ sample was carefully ground and the obtained powder was embedded in an epoxy glue. PXRD data were collected in the 2θ range of 10°–100° with a step size of 0.01°. The FullProf software package was used for Rietveld structure refinement [19] with the starting model reported in ref. [16] for $CePt_2In_7$.

Measurements of the magnetic susceptibility $\chi(T)$ were performed by using a Magnetic Property Measurement System (MPMS – Quantum Design) in the temperature range 3 K–300 K in an applied magnetic field of 7 T. A chunk of sample with a mass of 47.5 mg was glued inside a plastic holder. The data were corrected for the small paramagnetic signal of the sample holder.

The temperature dependence of electrical resistivity and heat capacity was measured using a Physical Property Measurement System (PPMS – Quantum Design). The electrical resistivity was determined using a standard four-contact dc technique, with four 50 μm diameter Pt wires connected to the flat polished sample by using silver epoxy (Epotek H20E). Magnetoresistance was measured with magnetic field of $\mu_0 H = 9$ T. The heat capacity was measured by using a relaxation method. Due to high radioactivity and toxicity of neptunium, the sample was embedded in the heat conducting STYCAST 2850 FT resin to avoid contamination risks. The raw heat capacity data were corrected by subtracting the signal estimated for the resin and for the Pt_3In_7 signal.

All technical operations were carried out in radioprotected glove boxes with low oxygen and water concentrations.

3. Experimental results

The room temperature PXRD pattern is shown in Fig. 1. Successful Rietveld refinement confirms that

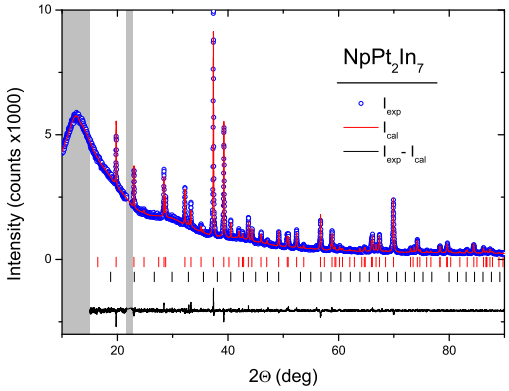

Figure 1: Rietveld refinement of room temperature powder X-ray diffraction data for $NpPt_2In_7$. Blue open circles (I_{exp}) and a red solid line (I_{cal}) represent observed and calculated data, respectively. Vertical tick marks are shown for two refined phases: $NpPt_2In_7$ (upper, red) and about 20% Pt_3In_7 impurity (lower, black). The differences between the observed and calculated pattern (I_{exp}-I_{obs}) are represented by a black line.

$NpPt_2In_7$ is an isostructural analogue of the rare-earth $CePt_2In_7$, with the model described in Ref. [16]. Extra PXRD lines seen in the pattern correspond to Pt_3In_7 (about 20% in weight). The used epoxy glue causes a large hump at low angle and a small peak at around 22°. Those regions were excluded for the Rietveld refinement. The crystallographic parameters and figures of merit derived from the fit are provided in Table 1.

Table 1: Refined structural parameters for $NpPt_2In_7$ at room temperature. Space group I4/mmm (s.g. #139), a = 4.58471(3) Å, c = 21.5065(3) Å. Calculated density 10.51 g cm^{-3}. Figures of merit: goodness of fit χ^2 = 1.48, weighted profile residual R_{wp} = 4.33%, profile residual R_p = 3.06%.

Atom	Position	z	B	Occ
Np	2b (0, 0, 0.5)		0.644(44)	1
Pt	4e (0, 0, z)	0.3257(1)	1.004(38)	1
In1	2a (0, 0, 0)		1.341(99)	1
In2	4d (0, 0.5, 0.25)		1.029(50)	1
In3	8g (0, 0.5, z)	0.1067(1)	1.274(46)	1

The lattice parameters and the unit cell volume for $NpPt_2In_7$ are larger than those previously reported for $PuPt_2In_7$ [18], and smaller than those reported for $CePt_2In_7$ [16] (see Table 2). The same trend is observed for a binary MIn_3 system, where M = Ce [20], Np [21] and Pu[22].

The magnetization $M(T)$ was measured under applied fields $\mu_0 H$ = 7 T and $\mu_0 H$ = 5 T, and the magnetic susceptibility χ was estimated as $\Delta M/\Delta H$. Its

MOST WIEDZY Downloaded from mostwiedzy.pl

Table 2: Unit cell parameters for $CePt_2In_7$ (Ref. [16]), $NpPt_2In_7$ (this work), and $PuPt_2In_7$ (Ref. [18]). The parameters for $CePt_2In_7$ and $PuPt_2In_7$ were obtained from single crystal x-ray diffraction collected at 173 K and at room temperature, respectively. Refined parameters for $NpPt_2In_7$ are based on room temperature powder x-ray diffraction.

	$CePt_2In_7$ [16]	$NpPt_2In_7$	$PuPt_2In_7$ [18]
a (Å)	4.5990(4)	4.58471(3)	4.5575(7)
c (Å)	21.580(2)	21.5065(3)	21.362(6)
V (Å^3)	456.4(1)	452.06(1)	443.7(3)

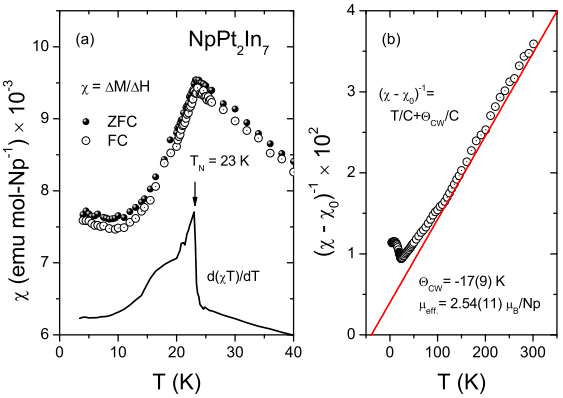

Figure 2: (a) Low temperature zero-field-cooling (ZFC) and field-cooling (FC) magnetic susceptibility for $NpPt_2In_7$. (b) Inverse magnetic susceptibility and a modified Curie–Weiss fit to the high temperature ($T > 100$ K) data.

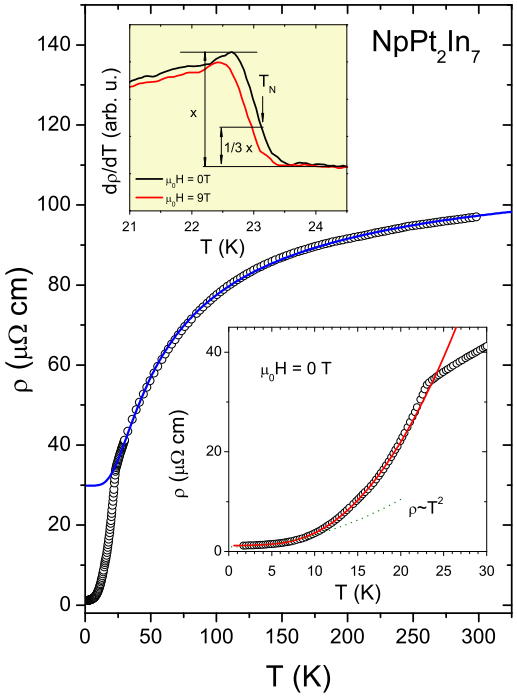

Figure 3: Temperature dependence of the electrical resistivity of $NpPt_2In_7$ measured in zero magnetic field. Black points are the experimental data, blue line is the fit with Equation 2 Top Inset: $d\rho(T)/dT$ in vicinity of the AFM transition measured under 0T and 9T applied magnetic field. Bottom Inset: Temperature dependence of the resistivity below T_N. The red solid curve is the fit to the data assuming the opening of a magnetic gap near T_N. The dashed green line is a low temperature fit with the Fermi liquid term.

temperature dependence, obtained after zero-field cooling (ZFC) and field-cooling (FC) from the paramagnetic phase, is shown in Fig. 2(a). The low temperature anomaly reveals the onset of antiferromagnetic order. An accurate value of the Néel temperature, $T_N = 23.0(5)$ K, is obtained from the maximum of the $d(\chi T)/dT$ curve [23, 24]. As shown in Fig. 2(a), the cooling history has negligible effects on the phase transition.

The inverse magnetic susceptibility $(\chi(T) - \chi_0)^{-1}$ in the T range 2 - 300 K is presented in Fig. 2(b). Above 100 K, the susceptibility follows a modified Curie–Weiss form:

$$\chi = \chi_0 + \frac{C}{T - \theta_{CW}}, \qquad (1)$$

where χ_0 is temperature independent susceptibility, C is the Curie constant and θ_{CW} is a Curie-Weiss temperature. The estimated fitting parameters are: $\theta_{CW} = -17 \pm 9$ K, and $C = 0.80 \pm 0.07$ emu K Np-mol^{-1}. Having C we can calculate the effective moment per Np from $\mu_{eff} = (8C)^{1/2} = 2.54 \pm 0.11\,\mu_B$. This value is close to $\mu_{eff} = 2.755\,\mu_B$ calculated for a trivalent Np^{3+} in the intermediate coupling scheme, and to $\mu_{eff} = 2.78\,\mu_B$ obtained for NpFeAsO oxypnictide material [24]. On the other hand, it is much larger than $\mu_{eff} = 1.5\,\mu_B$ reported for $NpCoGa_5$ [7]. The negative value of the Curie–Weiss temperature, $\theta_{CW} = -17$ K, might indicate the presence of antiferromagnetic interactions in $NpPt_2In_7$.

The temperature dependence of the electrical resistivity $\rho(T)$ is shown in Fig. 3. The measurement was performed in the temperature range from 1.8 K to 300 K, in zero applied magnetic field and with a current $I = 5$ mA. The $\rho(T)$ reveals metallic-like character ($d\rho/dT > 0$) with a sharp drop below 23 K, which is the onset of magnetic ordering. The $\rho(T)$ curve at temperatures above T_N has been fitted to the formula for the so-called

MOST WIEDZY Downloaded from mostwiedzy.pl

parallel resistor model (PRM):

$$\rho^{-1}(T) = \rho_{max}^{-1} + (\rho_0 + \rho_{BG})^{-1}, \quad (2)$$

where

$$\rho_{BG}(T) = 4R\theta_R \left(\frac{T}{\theta_R}\right)^5 \int_0^{\theta_R} \frac{x^5 dx}{(e^x - 1)(1 - e^{-x})}. \quad (3)$$

The model combines temperature independent resistors ρ_{max}, ρ_0, and a the Bloch-Grüneisen resistor represented by $\rho_{BG}(T)$. The residual resistivity $\rho_0 = 41\,\mu\Omega\,cm$ estimated from the fit is one order of magnitude larger than the resistivity measured in the antiferromagnetic state $\rho(2K) = 1\,\mu\Omega\,cm$. At high temperature, where the mean-free path approaches the interatomic distance, the resistivity starts saturating (Ioffe-Regel limit[25, 26]) to the estimated value of $\rho_{max} = 112\,\mu\Omega\,cm$. The last parameter in the fit is $\theta_R = 150$ K, the Debye temperature estimated from resistivity. The absence of any clear deviation of the resistivity curve from the fitted formula above T_N likely suggests the weakness of spin fluctuations in the paramagnetic regime.

The top inset (a) of Fig. 3 presents $d\rho/dT$ versus temperature in the vicinity of the transition. The Néel temperature was determined as 1/3 of the jump of $d\rho/dT$ [27]and is equal to $T_N = 23.1$ K under zero field and decreases to $T_N = 23.0$ K under $\mu_0 H = 9$ T, in perfect agreement with T_N obtained from magnetic susceptibility and heat capacity experiments.

The low-temperature resistivity data are presented in the bottom (b) inset of Fig. 3. The $\rho(T)$ curve cannot be fitted with the Fermi liquid term $\rho(T) = \rho_0 + AT^2$. Instead, the formula established for antiferromagnetic interactions with the opening of a magnetic gap [28] is found to successfully describe the low temperature resistivity, as demonstrated by a red solid line in top left Fig. 3:

$$\rho(T) = \rho_0 + aT^2 + bT\left(1 + \frac{2T}{\Delta}\right)\exp\left(-\frac{\Delta}{T}\right), \quad (4)$$

where $\rho_0 = 1.17\,\mu\Omega$cm, $a = 10.4(8)\,n\Omega$cmK^{-2}, $b = 1.29$ $\mu\Omega$cmK^{-1}, and $\Delta = 27(1)$ K.

Fig. 4 presents the Hall coefficient R_H for T= 2-100 K for $NpPt_2In_7$. R_H is slightly enhanced compared to common metals (Cu: 0.5×10^{-10} m^{3}C^{-1}) approaching 5.5×10^{-10} m^{3}C^{-1} at T_N, which is rather similar to values for neptunium intermetallic systems, e.g., NpIr and NpCoGe [29, 30]. When decreasing the temperature, R_H increases slightly but collapses below T_N= 23 K, saturating at low temperature at 1.0×10^{-10} m^{3}C^{-1}. As R_H is the result of the combination of the electron and hole

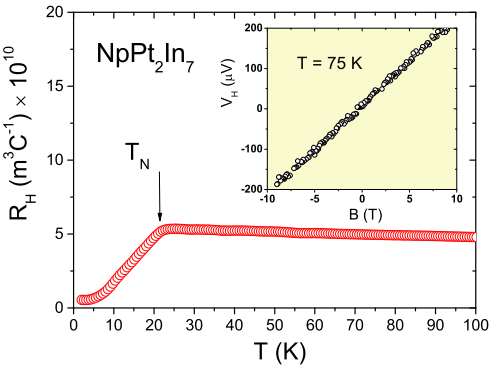

Figure 4: Temperature variation of the Hall Effect determined at 9 T from 2 to 100 K. The antiferromagnetic order is clearly visible at 23 K followed by a collapse of R_H below T_N while a small shoulder is marked around 17 K. In the paramagnetic state, Hall Effect is rising slowly when cooling down. Inset shows field dependence of V_H- Hall voltage - extracted perpendicular to the applied magnetic field on the sample at T= 75 K and showing a pure linear regime and a positive variation.

contributions with different carrier velocities and relaxation times, the sign conservation in the full temperature range of R_H suggests that the nature and the mobility of the carriers are not changing drastically in the paramagnetic state with temperature and only the antiferromagnetic order is impacting hole carriers below T_N. A simple one-band model then provides an estimation of 1.13×10^{28} m^{-3} for the concentration of free holes in the paramagnetic state giving an upper limit for the actual carrier concentration in $NpPt_2In_7$ converted into a rough estimate of 1.18 for the number of free holes per formula unit.

Fig. 5 presents the temperature dependence of the heat capacity (C_p) of $NpPt_2In_7$ corrected for the additional signal of the STYCAST and Pt_3In_7. Since the heat capacity for Pt_3In_7 was not reported, we grew single crystals of Pt_3In_7 and measured its C_P. At high temperature C_p saturates slightly above the expected Dulong–Petit value, $3nR \approx 250$ J mol^{-1} K^{-1}, where $n = 10$ is the number of atoms per formula unit and $R = 8.314$ J mol^{-1} K^{-1} is the gas constant.

A clear anomaly, shown in the inset of Fig. 5, confirms a bulk character of the AFM transition with T_N = 23 K in perfect agreement with magnetic susceptibility and transport results. It should be noted that the transition is very robust and the applied magnetic field only slightly suppresses the Néel temperature, i.e. T_N decreases by 0.2 K under 9 T.

We can describe heat capacity contributions at low temperature as $C_p = C_e + C_{phonons} + C_{mag}$, where $C_e = \gamma T$

MOST WIEDZY Downloaded from mostwiedzy.pl

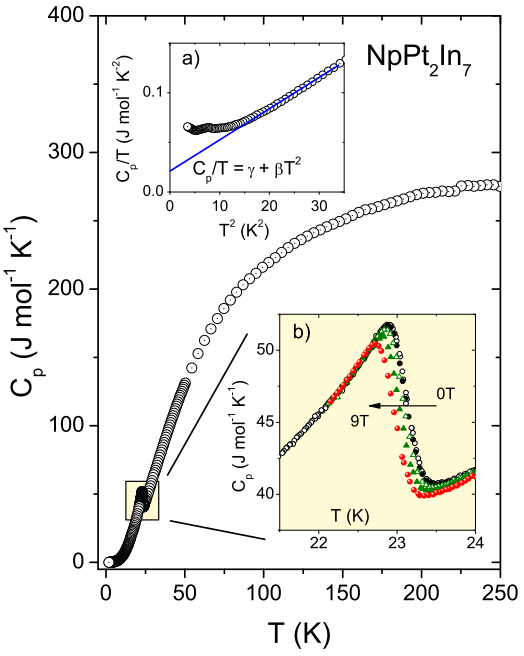

Figure 5: The specific heat versus temperature for $NpPt_2In_7$. Inset (a) shows the bulk antiferromagnetic transition with zero field and under applied magnetic field of $\mu_0 H$= 3 T, 6 T and 9 T. The bottom right inset shows C_p/T vs. T^2 plot with the fit $\gamma_e + \beta.T^2$ for the Sommerfeld linear coefficient determination and the Debye temperature estimation Θ_D.

corresponds to the electronic contribution of carriers, $C_{phonons} = \beta T^3$ lattice vibrations contribution at very low temperatures and C_{mag} takes into account antiferromagnetic interactions with the opening of a magnetic gap, following $aT^{1/2}\exp(-\Delta/T)$ behavior [31]. Inset (a) of Fig. 5 presents the C_p/T vs. T^2 behavior below 6 K. In this temperature range, typical magnetic contribution following previously quoted model of the antiferromagnetic interactions is negligible as Δ is generally of the same order of magnitude to T_N= 23 K, hence $C_{mag}/C_p < 1\%$ - and only phonons and electronic carriers contribute significantly to heat capacity. We extract γ= 24 $mJmol^{-1}K^{-2}$ and β= 3.28 $mJmol^{-1}K^{-4}$. Using Debye relation, we obtain an estimated Debye temperature Θ_D= 181 K, close to the 184 K reported for $CePt_2In_7$ single crystal [32] and 189 K for polycrystal [17]. This value is also similar to the resistivity Debye temperature θ_R= 150 K from the previously presented resistivity model. The observed upturn in C_p/T seen at the lowest temperature originates from the nuclear Schottky anomaly, which is often observed in Np compounds, e.g. $NpRh_2Sn$ [27], NpFeAsO [24], NpCoGa5 [7].

4. Electronic structure calculations

In order to theoretically analyze electronic structure and magnetic properties of $NpPt_2In_7$, we performed calculations in the framework of the correlated DFT+U method, an extension of the relativistic density functional theory (DFT), in which Coulomb-U and exchange-J are added to the correlated f-shell. We used the experimental crystal structure and a "state-of-the-art" full-potential linearized augmented plane-wave (FLAPW) basis set [33], taking into account both scalar-relativistic terms and spin-orbit coupling (SOC) implemented in the self-consistent second-variational procedure [34]. In the applied rotationally invariant implementation of the DFT+U including SOC [35, 36], all contributions to the f-manifold occupation matrix, including those nondiagonal in spin, are taken into account. The on-site Coulomb interaction in the correlated Np 5f shell is given by Slater integrals F_0 = 3.00 eV, F_2 = 7.43 eV, F_4 = 4.83 eV, and F_6 = 3.35 eV [37]. They correspond to commonly accepted values of Coulomb interaction U = 3 eV and exchange interaction J = 0.6 eV.

As a preliminary step, we performed spin-polarized DFT calculations in a local-spin density approximation (LSDA) including SOC, setting the magnetization on the Np atoms along the z-[001] axis (out-of-plane). As shown in Table 3, this approximation does not provide a satisfactory description of the experimental data, neither assuming a ferromagnetic (FM) arrangements on the Np magnetic moments nor an antiferromagnetic (AF) one. In both cases, the spin μ_S and orbital μ_L magnetic moments are aligned antiparallel to each other and are close in magnitude, so that the ensuing small value of the total magnetic moment $\mu_{tot} = \mu_S + \mu_L$ is not consistent with the experimental results.

A significant improvement on the predicted value for the total magnetic moment is obtained upon including many-body corrections by the DFT+U method. We performed these calculations using both the "around-mean-field" (AMF) and the "fully localized limit" (FLL) functionals for the double counting term, *i.e.* to subtract the correlation part from the DFT total energy. As seen from the results shown in Table 3, the DFT+U-FLL approximation fails to predict the observed AF ground state, as the calculated total energy difference between FM and AF configurations is negative (ΔE =

MOST WIEDZY Downloaded from mostwiedzy.pl

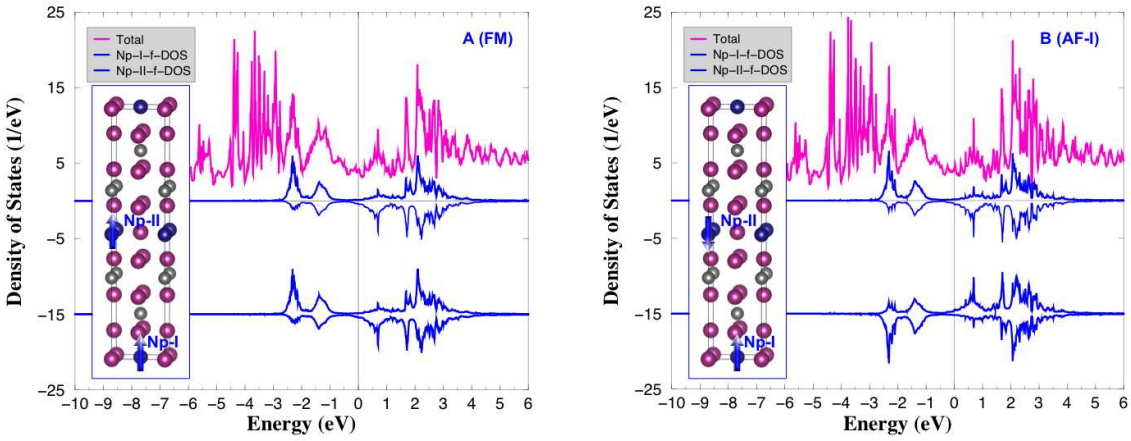

Figure 6: Total density of states (TDOS), and spin-resolved, f-projected DOS for the Np atoms in $NpPt_2In_7$ (A) in the FM case, (B) in the AF-I case, as obtained from the DFT+U-AMF calculations described in the text.

Table 3: Spin (μ_S), orbital (μ_L) and total magnetic moment ($\mu_{tot} = \mu_S + \mu_L$) in the units of μ_B for Np atom from DFT+SOC and DFT+U (in FLL and AFM versions) for the FM and AF Np atom arrangements, together with the total energy difference ΔE (in meV) between the FM and AF configurations.

	DFT+SOC		DFT+U-FLL		DFT+U-AMF	
	FM	AF	FM	AF	FM	AF
μ_S	3.48	3.48	3.20	3.20	1.37	1.38
μ_L	-3.16	-3.16	-5.20	-5.20	-4.19	-4.20
μ_{tot}	0.32	0.32	-2.0	-2.0	-2.82	-2.82
ΔE	4.2		-18.5		2.4	

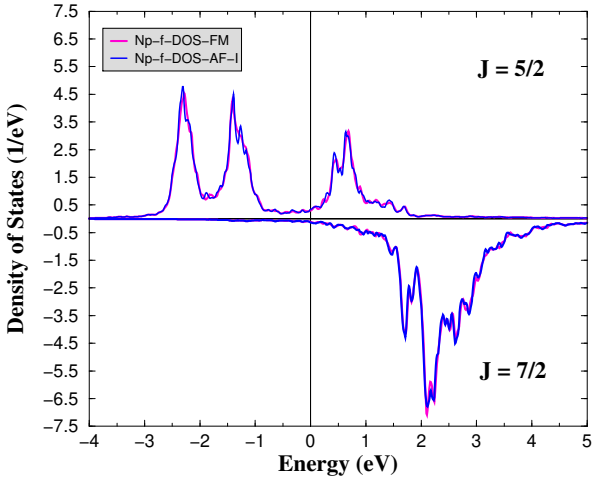

Figure 7: The J=5/2 and J=7/2 (shown as negative) f-projected DOS for the Np atoms in FM- and AF-I-$NpPt_2In_7$, as obtained from the DFT+U-AMF calculations.

-18.5 meV). On the contrary, in the DFT+U-AMF calculations the AF order is energetically favored, as ΔE = +2.4 meV.

The total magnetic moment obtained by DFT+U-AMF calculations is $|\mu_{tot}| = 2.82\ \mu_B$, very close to the experimental value of the effective paramagnetic moment $\mu_{eff} = 2.54 \pm 0.11\,\mu_B$. According to Rhodes-Wolfarth criterium [38], a ratio $|\mu_{tot}|/\mu_{eff}$ close to one suggests a rather localized character of the f-shell magnetic moments in $NpPt_2In_7$.

The total density of states (DOS), and the Np atom spin-resolved f-projected DOS are shown in Fig. 6. The effects of electron-electron interactions are responsible for the splitting of the occupied and unoccupied Np f-states, which have indeed a fairly localized character. The Np-f spin majority states are partially occupied and the spin minority ones are almost empty. The Np-f-states spin splitting is fairly similar in the FM and AF-I cases (see Fig. 6). The spin-orbit splitting of the Np-f-states is shown in Fig. 7, where the J=5/2 and J=7/2 f-projected DOS are shown for both the FM and AF-I cases. Again, as in the case of spin projected DOS shown in Fig. 6, the J-projected DOS are very similar. The Fig. 7 illustrates mainly J=5/2 character of the occupied f-manifold of the Np atom.

At the Fermi level, the total DOS of 4.0 1/eV per formula unit for the AF-I, and 3.94 1/eV for the FM cases are calculated. The total DOS includes the Np-f (0.54 1/eV), Pt-d (0.44 1/eV), and In-p (0.63 1/eV) contributions for the AF-I, and the Np-f (0.52 1/eV), Pt-d (0.40 1/eV), and In-p (0.49 1/eV) contributions for the FM cases.

The electronic specific heat coefficient γ can be es-

MOST WIEDZY Downloaded from mostwiedzy.pl

timated making use of the independent electron theory, $\gamma = \frac{\pi^2 k_B^2}{3} N(E_F)$, proportional to the DOS at the Fermi level, $N(E_F)$. This yields γ of 9.26 mJ K^{-2} per mole for the FM solution, and γ of 9.39 mJ K^{-2} per mole for the AF-I. The experimental Sommerfeld coefficient exceeds the theoretical estimate by a factor (1+λ)= 2.56. The λ enhancement originates from the electron-phonon interaction, and the spin fluctuations.

Furthermore, we computed the crystal-field matrix Δ_{CF} at the Np atomic site making use of the DFT+U local Green function as explained in Ref. [39]. Then we solved exactly the Anderson impurity hamiltonian [40] without hybridization, with the chemical potential given by the DFT+U f-occupation n_f=3.97 , the SOC parameter ξ = 0.26 eV, and the same Slater integrals as given above. We obtained the spin S=1.87, orbital L=5.84, and total J=4.01 moment quantum numbers, and the Landé factor g_J=0.64. This gives the value of 2.57 μ_B for Np f-shell effective moment, in a very good agreement with the experimental effective moment of μ_{eff}, and also supports the localized character of Np^{3+} in $NpPt_2In_7$.

The calculated Δ_{CF} matrix can be used to build the model crystal-field (CF) hamiltonian,

$$\hat{H}_{CF} = \sum_{kq} A_k^q \langle r^k \rangle \Theta_k(J) \hat{O}_k^q$$

where $\hat{O}_k^q$ are the Stevens operator equivalents, $\Theta_k(J)$ are the Stevens factors for a given ground state multiplet J, and $A_k^q\langle r^k\rangle$, the crystal field parameters (in standard notations) for given k and q.

The set of parameters $A_k^q\langle r^k\rangle$ is obtained by a least-square fit of Δ_{CF}. The calculated non-zero CF parameters $[A_k^q\langle r^k\rangle]$ for Np atom in $NpPt_2In_7$ are shown in Table 4 in the AF-I case. Note that the CF parameters remain very similar in the FM case.

Table 4: The non-zero CF parameters $[A_k^q\langle r^k\rangle]$ (meV) for Np atom in $NpPt_2In_7$ calculated in the AF-I case.

	$A_2^0\langle r^2\rangle$	$A_4^0\langle r^4\rangle$	$A_4^4\langle r^4\rangle$	$A_6^0\langle r^6\rangle$	$A_6^4\langle r^6\rangle$
CF (meV)	-28.85	-14.6	14.8	2.1	-234.1

So far, we have considered the direction of the magnetic moment along the z-[001] axis. In reality, it is determined by the magnetic anisotropy energy (MAE), and for the uniaxial crystal symmetry the MAE reads, $E_A \approx K_1 \sin^2\theta$, where θ is the angle between the magnetization and the z-[001] axis, and K_1 is the first-order anisotropy constant. An accurate total energy theoretical determination of K_1 for $NpPt_2In_7$ would be numerically a very demanding task. Assuming that, like in the rare-earth intermetallics, the MAE is dominated by the Np single-ion contribution, we can use the expression [41],

$$K_1 = -3J(J - \frac{1}{2})\Theta_2(J) A_2^0 \langle r^2 \rangle$$

for the semi-quantitative MAE estimate. It yields K_1=9.3 meV per Np for the AF-I case, and K_1=9.6 meV/Np for the FM case. The positive sign of the MAE indicates the easy axis is indeed z-[001].

A recent neutron diffraction experiment revealed a two-dimensional magnetic ordering for the isostructural $CePt_2In_7$ compound [42]. Since the crystal structure of both materials is the same, it is plausible to expect some similarities in their magnetic properties and to assume that a layered magnetic superlattice appears below T_N also in the three dimensional bulk $NpPt_2In_7$. In analogy with $CePt_2In_7$, it is reasonable to assume the formation of an in-plane checkerboard AF arrangement. In a body centered tetragonal crystal structure the actual magnetic order of the AF planes along the z-[001] axis will be determined by competition of very weak interlayer interactions, as indeed suggested by the small energy difference between the FM and AF configurations (see Table 3). Also, it opens a possibility for metamagnetic transitions in the external field, which can play an important role for the occurrence of the giant magnetoresistance. We emphasize that a direct determination of the magnetic structure by neutron diffraction on a single crystal of $NpPt_2In_7$ would be essential to explore this phenomenon further.

5. Conclusions

Our results indicate that $NpPt_2In_7$ is a metallic antiferromagnet with a prevalently localized character of the Np magnetic moment, similarly to $NpGoGa_5$ [8]. The compound orders magnetically at T_N = 23 K, which was confirmed by all performed experiments. From the magnetic susceptibility measurements, we estimated the Curie–Weiss temperature $\theta_{CW} = -17 \pm 9$ K and the effective magnetic moment in the paramagnetic phase as $\mu_{eff} = 2.54 \pm 0.11\,\mu_B$, which is close to the value calculated for trivalent neptunium in intermediate coupling scheme. Finally, we presented the results of a theoretical investigation of the compound, by means of correlated band theory DFT+U method. The calculations show very weak anti-ferromagnetic interlayer coupling between different Np-layers along the

MOST WIEDZY Downloaded from mostwiedzy.pl

z-[001] axis, and suggest localized magnetic moments and a positive uniaxial anisotropy. We propose that the actual magnetic structure shows an in-plane checkerboard AF arrangement. We notice that in presence of local moments in a quasi-two-dimensional antiferromagnetic structure a positive and large magnetoresistance could emerge if the external magnetic field promotes the formation of short-range antiferromagnetically correlated regions embedded in a field-induced ferromagnetic background. This has recently been predicted to occur in double perovskite systems [43] and observed in half-metallic double-perovskite Sr_2CrWO_6 thin films[44]. $NpPt_2In_7$ could be a physical realization of such an uncommon phenomenon and we plan to investigate it once a single crystal specimen will become available.

6. Acknowledgments

This work has been performed at the at the Joint Research Centre within its Actinide User Laboratory program, with financial support to users provided by the European Commission. The Np metal required for the fabrication of the compound was made available through a loan agreement between Lawrence Livermore National Laboratory and the Joint Research Centre in the framework of a collaboration involving Lawrence Livermore National Laboratory, Los Alamos National Laboratory, and the US Department of Energy. This work was supported by the National Science Centre (Poland) grant No. DEC-2015/17/N/ST3/03790, by Operational Programme Research, Development and Education financed by European Structural and Investment Funds and the Czech Ministry of Education, Youth and Sports (Project No. SOLID21 - CZ.02.1.01/0.0/0.0/16-019/0000760), and by the Czech Science Foundation (GACR) grant No. 18-06240S. A.K. acknowledge the TASK Academic Computer Centre (Gdansk, Poland). Access to computing and storage facilities of the National Grid Infrastructure MetaCentrum provided under the programme "Projects of Projects of Large Research, Development, and Innovations Infrastructures" (CESNET LM2015042), is acknowledged.

References

[1] C. Petrovic, P. G. Pagliuso, M. F. Hundley, R. Movshovich, J. L. Sarrao, J. D. Thompson, Z. Fisk, P. Monthoux, Heavy-fermion superconductivity in $CeCoIn_5$ at 2.3 k, Journal of Physics: Condensed Matter 13 (17) (2001) L337.

[2] C. Petrovic, R. Movshovich, M. Jaime, P. G. Pagliuso, M. F. Hundley, J. L. Sarrao, Z. Fisk, J. D. Thompson, A new heavy-fermion superconductor ceirin 5 : A relative of the cuprates?, EPL (Europhysics Letters) 53 (3) (2001) 354.

[3] H. Hegger, C. Petrovic, E. G. Moshopoulou, M. F. Hundley, J. L. Sarrao, Z. Fisk, J. D. Thompson, Pressure-induced superconductivity in quasi-2d $CeRhIn_5$, Phys. Rev. Lett. 84 (2000) 4986–4989. doi:10.1103/PhysRevLett.84.4986.

[4] D. Kaczorowski, A. P. Pikul, D. Gnida, V. H. Tran, Emergence of a superconducting state from an antiferromagnetic phase in single crystals of the heavy fermion compound Ce_2PdIn_8, Phys. Rev. Lett. 103 (2009) 027003. doi:10.1103/PhysRevLett.103.027003.

[5] M. Kratochvilova, M. Dusek, K. Uhlirova, A. Rudajevova, J. Prokleska, B. Vondrackova, J. Custers, V. Sechovsky, Single crystal study of the layered heavy fermion compounds ce_2pdin_8, ce_3pdin_11, ce_2ptin_8 and ce_3ptin_11, Journal of Crystal Growth 397 (2014) 47 – 52. doi:http://dx.doi.org/10.1016/j.jcrysgro.2014.04.008.

[6] E. D. Bauer, M. M. Altarawneh, P. H. Tobash, K. Gofryk, O. E. Ayala-Valenzuela, J. N. Mitchell, R. D. McDonald, C. H. Mielke, F. Ronning, J.-C. Griveau, E. Colineau, R. Eloirdi, R. Caciuffo, B. L. Scott, O. Janka, S. M. Kauzlarich, J. D. Thompson, J. Phys. Condens. Matter 24 (2012) 052206.

[7] E. Colineau, P. Javorský, P. Boulet, F. Wastin, J. C. Griveau, J. Rebizant, J. P. Sanchez, G. R. Stewart, Magnetic and electronic properties of the antiferromagnet $NpCoGa_5$, Phys. Rev. B 69 (2004) 184411. doi:10.1103/PhysRevB.69.184411.

[8] N. Magnani, A. Hiess, R. Caciuffo, E. Colineau, F. Wastin, J. Rebizant, G. H. Lander, Magnetic excitations in $npcoga_5$: Inelastic neutron scattering experiments, Phys. Rev. B 76 (2007) 100404.

[9] B. Detlefs, S. B. Wilkins, R. Caciuffo, J. A. Paixão, K. Kaneko, F. Honda, N. Metoki, N. Bernhoeft, J. Rebizant, G. H. Lander, Resonant x-ray scattering study of $NpRhga_5$ and $NpCoga_5$, Phys. Rev. B 77 (2008) 024425.

[10] D. Aoki, Y. Haga, Y. Homma, Y. Shiokawa, E. Yamamoto, A. Nakamura, R. Settai, Y. Ōnuki, Magnetic properties and heavy electronic states in the antiferromagnet npptga5, Journal of the Physical Society of Japan 75 (11) (2006) 114715. doi:10.1143/JPSJ.75.114715.

[11] D. Aoki, Y. Haga, T. D. Matsuda, N. Tateiwa, S. Ikeda, Y. Homma, H. Sakai, Y. Shiokawa, E. Yamamoto, A. Nakamura, R. Settai, Y. Ōnuki, Unconventional heavy-fermion superconductivity of a new transuranium compound $NpPd_5Al2$, Journal of the Physical Society of Japan 76 (6) (2007) 063701. doi:10.1143/JPSJ.76.063701.

[12] H. Chudo, H. Sakai, Y. Tokunaga, S. Kambe, D. Aoki, Y. Homma, Y. Shiokawa, Y. Haga, S. Ikeda, T. D. Matsuda, Y. Ōnuki, H. Yasuoka, ^{27}Al NMR evidence for the strong-coupling d-wave superconductivity in $NpPd_5Al_2$, Journal of the Physical Society of Japan 77 (8) (2008) 083702. doi:10.1143/JPSJ.77.083702.

[13] K. Gofryk, J.-C. Griveau, E. Colineau, J. P. Sanchez, J. Rebizant, R. Caciuffo, Kondo behavior in superconducting nppd5al2, Phys. Rev. B 79 (2009) 134525. doi:10.1103/PhysRevB.79.134525.

[14] G. A. Ummarino, R. Caciuffo, H. Chudo, S. Kambe, Energy scale of the electron-boson spectral function and superconductivity in $nppd_5al_2$, Phys. Rev. B 82 (2010) 104510.

[15] D. Damien, C. de Novion, J. Gal, Superconductivity in the neptunium chevrel phase np1+xmo6se8, Solid State Communications 38 (5) (1981) 437 – 440. doi:http://dx.doi.org/10.1016/0038-1098(81)90274-X.

[16] T. Klimczuk, O. Walter, L. Müchler, J. W. Krizan, F. Kinnart, R. J. Cava, Crystal structure and electronic structure of $CePt_2In_7$, Journal of Physics: Condensed Matter 26 (40) (2014) 402201.

[17] E. D. Bauer, H. O. Lee, V. A. Sidorov, N. Kurita, K. Gofryk,

MOST WIEDZY Downloaded from mostwiedzy.pl

J.-X. Zhu, F. Ronning, R. Movshovich, J. D. Thompson, T. Park, Pressure-induced superconducting state and effective mass enhancement near the antiferromagnetic quantum critical point of $CePt_2In_7$, Phys. Rev. B 81 (2010) 180507. doi:10.1103/PhysRevB.81.180507.

[18] H. B. Rhee, F. Ronning, J.-X. Zhu, E. D. Bauer, J. N. Mitchell, P. H. Tobash, B. L. Scott, J. D. Thompson, Y. Jiang, C. H. Booth, W. E. Pickett, $PuPt_2In_7$: A computational and experimental investigation, Phys. Rev. B 86 (2012) 115137. doi:10.1103/PhysRevB.86.115137.

[19] J. Rodriguez-Carvajal, FULLPROF: A program for Rietveld refinement and pattern matching analysis, in: Abstracts of the Satellite Meeting on Powder Diffraction of the XV Congress of the IUCr, Toulouse, France, 1990, p. 127.

[20] E. G. Moshopoulou, R. M. Ibberson, J. L. Sarrao, J. D. Thompson, Z. Fisk, Structure of Ce_2RhIn_8: an example of complementary use of high-resolution neutron powder diffraction and reciprocal-space mapping to study complex materials, Acta Crystallographica Section B 62 (2) (2006) 173–189. doi:10.1107/S0108768106003314.
URL `https://doi.org/10.1107/S0108768106003314`

[21] J. Gal, I. Yaar, S. Fredo, I. Halevy, W. Potzel, S. Zwirner, G. M. Kalvius, Magnetic and electronic properties of cubic npx_3 intermetallics, Phys. Rev. B 46 (1992) 5351–5356. doi:10.1103/PhysRevB.46.5351.

[22] F. Ellinger, C. Land, K. Johnson, The plutonium-indium system, Transactions of the metallurgical society of AIME.

[23] P. Dutta, M. S. Seehra, S. Thota, J. Kumar, A comparative study of the magnetic properties of bulk and nanocrystalline Co_3O_4, Journal of Physics: Condensed Matter 20 (1) (2008) 015218.

[24] T. Klimczuk, H. C. Walker, R. Springell, A. B. Shick, A. H. Hill, P. Gaczyński, K. Gofryk, S. A. J. Kimber, C. Ritter, E. Colineau, J.-C. Griveau, D. Bouëxière, R. Eloirdi, R. J. Cava, R. Caciuffo, Negative thermal expansion and antiferromagnetism in the actinide oxypnictide NpFeAsO, Phys. Rev. B 85 (2012) 174506. doi:10.1103/PhysRevB.85.174506.

[25] N. H. , K. Takenaka, H. Takagi, Universality of the mottiofferegel limit in metals, Philosophical Magazine 84 (27) (2004) 2847–2864. doi:10.1080/14786430410001716944.

[26] A. F. Ioffe, A. R. Regel, Non-crystalline, amorphous, and liquid electronic semiconductors, Prog. Semicond. 4 (1960) 237–291.

[27] T. Klimczuk, J.-C. Griveau, P. Gaczyński, R. Eloirdi, E. Colineau, R. Caciuffo, Crystal structure and physical properties of nprh 2 sn, a new np-based ternary compound, Journal of Physics: Conference Series 273 (1) (2011) 012024.

[28] N. H. Andersen, Electrical resistivity investigations on metallic rare-earths, in: J. E. Crow, R. P. Guertin, T. W. Mihalisin (Eds.), Crystalline Electric Field and Structural Effects in f-Electron Systems, Springer US, 1980, pp. 373–387.

[29] H. C. Walker, K. A. McEwen, J.-C. Griveau, R. Eloirdi, P. Amador, P. Maldonado, P. M. Oppeneer, E. Colineau, Magnetic, electrical, and thermodynamic properties of npir: Ambient and high-pressure measurements, and electronic structure calculations, Phys. Rev. B 91 (2015) 195146. doi:10.1103/PhysRevB.91.195146.

[30] E. Colineau, J.-C. Griveau, R. Eloirdi, P. Gaczyński, S. Khmelevskyi, A. B. Shick, R. Caciuffo, Antiferromagnetic ground state in npcoge, Phys. Rev. B 89 (2014) 115135. doi:10.1103/PhysRevB.89.115135.

[31] N. H. Andersen, H. Smith, Electron-magnon interaction and the electrical resistivity of tb, Phys. Rev. B 19 (1979) 384–387. doi:10.1103/PhysRevB.19.384.

[32] P. H. Tobash, F. Ronning, J. D. Thompson, B. L. Scott, P. J. W. Moll, B. Batlogg, E. D. Bauer, Single crystal study of the heavy-fermion antiferromagnet $CePt_2In_7$, Journal of Physics: Condensed Matter 24 (1) (2012) 015601.

[33] E. Wimmer, H. Krakauer, M. Weinert, A. J. Freeman, Full-potential self-consistent linearized-augmented-plane-wave method for calculating the electronic structure of molecules and surfaces: O_2 molecule, Phys. Rev. B. 24 (1981) 864. doi:10.1103/PhysRevB.24.864.

[34] A. B. Shick, D. L. Novikov, A. J. Freeman, Relativistic spin-polarized theory of magnetoelastic coupling and magnetic anisotropy strain dependence: Application to Co/Cu(001), Phys. Rev. B 56 (1997) R14259–R14262.

[35] A. B. Shick, W. E. Pickett, Magnetism, spin-orbit coupling, and superconducting pairing in UGe_2, Phys. Rev. Lett. 86 (2001) 300–303.

[36] A. B. Shick, V. Drchal, L. Havela, Europhys. Lett 69 (2005) 588.

[37] K. T. Moore, G. van der Laan, Nature of the 5f states in actinide metals, Rev. Mod. Phys. 81 (2009) 235–298.

[38] Y. Izymov, M. Katsnelson, Y. Skryabin, Itinerant electron magnetism, Moskow, "Nauka" (in Russian), 1993.

[39] A. Shick, D. Shapiro, J. Kolorenč, A. Lichtenstein, Scientific Reports 7 (2017) 2752.

[40] A. Hewson, The Kondo Problem to Heavy Fermions, Cambridge University Press, 1993.

[41] M. Richter, P. M. Oppeneer, H. Eschrig, B. Johansson, Phys. Rev. B 46 (1992) 13919.

[42] M. Raba, E. Ressouche, N. Qureshi, C. V. Colin, V. Nassif, S. Ota, Y. Hirose, R. Settai, P. Rodière, I. Sheikin, Determination of the magnetic structure of $cept_2in_7$ by means of neutron diffraction, Phys. Rev. B 95 (2017) 161102. doi:10.1103/PhysRevB.95.161102.

[43] V. N. Singh, P. Majumdar, J. Phys. Condens. Matter 26 (2014) 296001.

[44] J. Zhang, W.-J. Ji, J. Xu, X.-Y. Geng, J. Zhou, Z.-B. Gu, S.-H. Yao, S.-T. Zhang, Giant positive magnetoresistance in half-metallic double-perovskite sr2crwo6 thin films, Science Advances 3 (2017) e1701473.

MOST WIEDZY Downloaded from mostwiedzy.pl